

## Accepted Manuscript

Title: Assessing the potential of quartz crystal microbalance to estimate water vapor transfer in micrometric size cellulose particles

Authors: Valentin Thoury-Monbrun, Sébastien Gaucel, Vincent Rouessac, Valérie Guillard, Hélène Angellier-Coussy



PII: S0144-8617(18)30226-1  
DOI: <https://doi.org/10.1016/j.carbpol.2018.02.068>  
Reference: CARP 13330

To appear in:

Received date: 9-11-2017  
Revised date: 21-2-2018  
Accepted date: 22-2-2018

Please cite this article as: Thoury-Monbrun, Valentin., Gaucel, Sébastien., Rouessac, Vincent., Guillard, Valérie., & Angellier-Coussy, Hélène., Assessing the potential of quartz crystal microbalance to estimate water vapor transfer in micrometric size cellulose particles. *Carbohydrate Polymers* <https://doi.org/10.1016/j.carbpol.2018.02.068>

This is a PDF file of an unedited manuscript that has been accepted for publication. As a service to our customers we are providing this early version of the manuscript. The manuscript will undergo copyediting, typesetting, and review of the resulting proof before it is published in its final form. Please note that during the production process errors may be discovered which could affect the content, and all legal disclaimers that apply to the journal pertain.

## Assessing the potential of quartz crystal microbalance to estimate water vapor transfer in micrometric size cellulose particles

Valentin Thoury-Monbrun <sup>a</sup>, Sébastien Gaucel <sup>a</sup>, Vincent Rouessac <sup>b</sup>, Valérie Guillard <sup>a</sup>, Hélène Angellier-Coussy <sup>a</sup>

*a* JRU IATE 1208 – CIRAD/INRA/Montpellier Supagro/University of Montpellier, 2 Place Pierre Viala, Bat 31, F-34060 Montpellier 01, France

*b* IEM ENSCM/UM/CNRS UMR 5635, Université de Montpellier, 2 Place Eugène Bataillon, 34095 Montpellier cedex 05, France

[valentin.thoury@supagro.fr](mailto:valentin.thoury@supagro.fr)

[sebastien.gaucel@inra.fr](mailto:sebastien.gaucel@inra.fr)

[vincent.rouessac@umontpellier.fr](mailto:vincent.rouessac@umontpellier.fr)

[valerie.guillard@umontpellier.fr](mailto:valerie.guillard@umontpellier.fr)

[helene.coussy@umontpellier.fr](mailto:helene.coussy@umontpellier.fr)

Corresponding author: Hélène Angellier-Coussy, [helene.coussy@umontpellier.fr](mailto:helene.coussy@umontpellier.fr), +33 (0)499612432, UMR 1208 IATE - 2 place Viala - bât. 31 F-34060 Montpellier Cedex 01

### Highlights

- QCM allows measuring water vapor transfer in a micrometric cellulose particle.
- Water vapor kinetics was successfully achieved on 1 µg of cellulose.
- Water vapor diffusivity and sorption were estimated from analytical solutions.
- Diffusivity ranges from  $2.2 \times 10^{-14}$  to  $3.3 \times 10^{-13}$  m<sup>2</sup>.s<sup>-1</sup> for RH from 0 to 90%.
- Cylinder or spherical geometry can be equally used for aspect ratio lower than 2.

### Abstract

This study aims at assessing the use of a quartz crystal microbalance (QCM) coupled with an adsorption system to measure water vapor transfer properties in micrometric size cellulose particles. This apparatus allows measuring successfully water vapor sorption kinetics at successive relative humidity (RH) steps on a dispersion of individual micrometric size cellulose particles (1 µg) with a total acquisition duration of the order of one hour. Apparent diffusivity and water uptake at equilibrium were estimated at each step of RH by considering two different particle geometries in mass transfer modeling, i.e. sphere or finite cylinder, based on the results obtained from image analysis. Water vapor diffusivity values varied from  $2.4 \times 10^{-14}$  m<sup>2</sup>.s<sup>-1</sup> to  $4.2 \times 10^{-12}$  m<sup>2</sup>.s<sup>-1</sup> over the tested RH range (0 to 80%) whatever the model used. A finite cylinder or spherical geometry could be used equally for diffusivity identification for a particle size aspect ratio lower than 2.

Keywords: Vegetal particle; Quartz Crystal Microbalance; Morphological analysis; Sorption; Diffusion coefficient; Water vapor

## 1. Introduction

The use of biocomposites based on a fully biosourced and biodegradable polymer matrix combined with micrometric size cellulose or lignocellulose-based fillers is gaining more and more attention in the field of food packaging. They constitute an answer to both environmental and socio-economical concerns by reducing our dependence to oil resources, decreasing environmental pollution while displaying specific new functionalities allowing to better preserve food products (Marie-Alix Berthet, Angellier-Coussy, Guillard, & Gontard, 2016). Considering this field of application, the key material properties that should be tailored and controlled are mass transfer properties. Mass transfers are characterized by two main phenomena, sorption and diffusion, characterized by the sorption coefficient, which is a thermodynamic parameter, and the diffusion coefficient or diffusivity, which is a kinetic parameter. In front of the diversity of the implied materials and keeping in mind the objective of designing in a reasoned way packaging material, the mathematical modeling of the link between structure and mass transfer properties in biocomposites is essential. However, there is still currently a gap of knowledge regarding the formalization of these relationships due to the difficulty to characterize mass transfer properties in two of the three compartments of composite structures, i.e. the filler/matrix interphase and the fillers themselves. Indeed, mass transfer properties are well-known in neat polymer matrices and can be easily measured in the whole biocomposite material (M.-A. Berthet, Gontard, & Angellier-Coussy, 2015; de Carvalho et al., 2016; Gouanvé, Marais, Bessadok, Langevin, & Métayer, 2007). Efforts have been made to characterize mass transfer properties in cellulose or lignocellulose-based materials and mainly focused on water vapor transfers. Many studies have been devoted to the study of water vapor sorption kinetics, for all kinds of cellulose or lignocellulose-based materials and even on micrometric size particles, as reported by Paes et al. for ball milled cellulose (Paes et al., 2010). However, measurements were all carried out on sample weights higher than 1 mg and/or stacks of particles, which may not be representative of phenomenon occurring at the level of an individual particle. Different gravimetric methodologies can be found in literature to measure water vapor sorption kinetics, i.e. isopiestic methods such as the use of salt saturated solutions (Mihriyan, Llagostera, Karmhag, Strømme, & Ek, 2004), Dynamic Vapor Sorption (DVS) using a Cahn microbalance (Paes et al., 2010) or Intelligent Gravimetric Analyzer (IGA) (Gouanvé et al., 2006). In the case of simple geometries, i.e. finite or infinite cylinders, spheres or infinite plates, analytical solutions of Fick's law allowed the estimation of the apparent diffusivity from sorption kinetics (Guillard, Broyart, Bonazzi, Guilbert, & Gontard, 2003; Marais et al., 2000). This requires an accurate evaluation of the particle morphology or to make an assumption in order to select the appropriate analytical solution. Most published studies on diffusivity estimation are focusing either on long fibre bundles with a length higher than 1 cm, such as flax, hemp, jute, sisal (Céline, Fréour, Jacquemin, & Casari, 2013) or agave fibres (Bessadok et al., 2009), sheets of associated fibres such as papers or films (Li, Henriksson, Klason, & Ödberg, 1992; Minelli et al., 2010), or pieces of raw biomasses such

as wheat straw (Wolf, Guillard, Angellier-Coussy, Silva, & Gontard, 2016), raffia (Tiaya Mbou, Njeugna, Kemajou, Sikame, & Ndapeu, 2017) or wood (Khazaei, 2008; Simpson, 1993), but never on individual micrometric size particles. Furthermore, it is worth noting that for a given material, a large range of water vapor diffusivity values have been reported. As an example, water vapor diffusivity of a paper sheet could vary from  $3 \cdot 10^{-12}$  to  $4 \cdot 10^{-7} \text{ m}^2 \cdot \text{s}^{-1}$  (Bedane, Huang, Xiao, & Ei, 2012; Hashemi, Comes, Crotogino, & Douglas, 1997; Nilsson, Wilhelmsson, & Stenstrom, 1993), depending on the paper composition, chosen methodology and modeling approach. As another example, water vapor diffusivity of lignocellulosic fibres (agave fibres with length of the order of centimeter) could vary from  $8 \cdot 10^{-10}$  to  $2 \cdot 10^{-8} \text{ m}^2 \cdot \text{s}^{-1}$  according to modeling approach and relative humidity (Bessadok et al., 2009). This highlights the complexity of accurately assessing mass transfer properties in cellulose or lignocellulose-based particles and the lack of reference method. Furthermore, for all these studies, identified diffusivities were only estimated for either macroscopic samples or beds of particles that never represent the diffusion within one micrometric size particle.

Quartz crystal microbalance (QCM) is an extremely sensitive technique able to detect a mass of  $7 \cdot 10^{-7} \mu\text{g}$  in the best case (Stockbridge, Warner, & Behrndt, 1963), mostly depending on the frequency stability. This minimal detection load has to be compared with that of the most sensitive classical balances, i.e.  $0.1 \mu\text{g}$  (Mecea, 2006). This technique is well known to follow the thickness of a deposited layer during its growth in a vacuum deposition technique, knowing the mass density of the deposited material. During the last years, the QCM has been extensively used as a sensor devoted to the study of the detection of numerous biomolecules (Villares, Moreau, Dammak, Capron, & Cathala, 2015), to analyze selective membranes and sensors to a specific gas (Caron et al., 2014; Jia, Yu, Zhang, Dong, & Li, 2016; Michalzik, Wilke, & Büttgenbach, 2005; Passamano & Pighini, 2006) and to evaluate interfacial polymer behavior (Ahola, Myllytie, Österberg, Teerinen, & Laine, 2008; Marx, 2003; Tammelin et al., 2015). QCM with dissipation monitoring (QCM-D) could be useful to investigate viscoelastic properties of the adsorbed layer and take into consideration energy dissipation effects (Hakalahti, Faustini, Boissière, Kontturi, & Tammelin, 2017; Kontturi, Kontturi, & Laine, 2013; Niinivaara, Faustini, Tammelin, & Kontturi, 2015, 2016). Up to now, QCM has mainly been used for thin films, generally deposited by spin coating (Kushner & Hickner, 2017; Rouessac, van der Lee, Bosc, Durand, & Ayrat, 2008; Thomas, Rudich, Trakhtenberg, & Ussyshkin, 1999). A study has been carried out on the use of QCM-D to determine the equilibrium water content inside cellulose nanofibers prepared by electrospinning by regenerating cellulose to obtain a thin cellulose film (to keep fibers of QCM sensor) (Roemhild et al., 2016). However, no work has been yet proposed to measure mass variations of dispersed micrometric size powders or fibres.

In this context, the aim of this work is to explore the potential of using the QCM coupled with a water vapor adsorption/desorption system as a reliable methodology to evaluate water vapor transfer (apparent diffusivity and sorption) in individual micrometric size cellulose particles from water vapor kinetics recorded at different relative humidities, which is never possible with classical methods. For

this purpose, pure cellulose was selected. After having discussed the suitability of the QCM system, the paper focuses on evaluating the impact of the hypothesis for sample geometry on the estimation of water vapor diffusivity by a comparison of two analytical solutions. This choice was critically done based on the characterization of particle morphology (size and shape- through both laser diffraction granulometry and image analysis).

## 2. Materials and methods

### 2.1. Materials

Arbocel® BE 600-10 Tg cellulose was provided by J. Rettenmaier & Söhne (JRS). According to the manufacturer, it was highly pure cellulose (cellulose content of 99.5 wt%) with an average fibre length of 18  $\mu\text{m}$ , an average fibre thickness of 15  $\mu\text{m}$  and a bulk density around 0.23 – 0.30  $\text{g}\cdot\text{cm}^{-3}$ , obtained after successive grinding and sorting steps from pine cellulose pulp. The true density of cellulose, measured by pycnometry, was 1.56  $\text{g}\cdot\text{cm}^{-3} \pm 0.08$ . Crystallinity of cellulose was determined using a Philips PW3830 generator, results shown that cellulose is quasi amorphous (crystallinity less than 5%). Absolute ethanol (purity of 99.9 %) was purchased from Meridis (France). Gold sensor crystals with nominal frequency equal to 6 MHz were supplied by Neyco (France).

### 2.2. Methods

#### 2.2.1. Water vapor sorption kinetics using a quartz crystal microbalance coupled with adsorption

**Quartz preparation.** First, the peripheral unusable surface of a golden AT-cut quartz resonator was masked by putting a tape. Then, 15  $\mu\text{L}$  of a suspension of cellulose in absolute ethanol at a concentration of 0.07  $\text{g}\cdot\text{L}^{-1}$  was deposited on the usable surface ( $S = 0.5 \text{ cm}^2$ ) of the quartz resonator in order to obtain a total weight of cellulose ranging from 1 to 1.5  $\mu\text{g}$ . Ethanol was then evaporated under vacuum. The goal of this preparation was to achieve the best repeatability of data. The weight of one cellulose particle being around  $5.7 \times 10^{-4} \mu\text{g}$  (value deduced from the true density of particles and the average size given by the supplier), it was calculated from the total deposited weight that around 2000 particles were deposited on each quartz.

**Water vapor sorption kinetics.** Water vapor sorption kinetics were carried out using a QCM apparatus (Maxtek TM-400). Frequency variation  $\Delta f$  was measured by this apparatus.  $\Delta f$  is the difference between the frequency of the quartz at time  $t$  and the frequency of the quartz at time  $t_0$ , in MHz. This frequency variation was linked to mass variation due to water vapor sorption or desorption.  $\Delta f$  is proportional to the mass variation of quartz  $\Delta m$  according to Sauerbrey equation Eq. (1) (Rouessac et al., 2008) :

$$\Delta f = -\frac{f_q^2 \cdot \Delta m}{C \cdot \rho_q \cdot S} \quad (1)$$

where  $f_q$  is the nominal frequency (6 MHz) of the quartz, value depending on its size,  $\rho_q = 2.65 \text{ g.cm}^{-3}$  the quartz density,  $S$  the usable area ( $0.5 \text{ cm}^2$ ) of quartz where cellulose particles were deposited and  $C$  an apparatus constant ( $1.67 \times 10^5 \text{ cm.s}^{-1}$ ).

Initial sample weight was determined by measuring the frequencies difference between the pristine dry quartz and the quartz loaded by the cellulose. In this paper, knowing that mass of quartz and cellulose were constant,  $\Delta m$  corresponded to the water mass uptake  $m_{\text{sorbed}}$  ( $\mu\text{g}$ ) of cellulose particles.

Cellulose particles were adsorbed on a golden AT-cut quartz resonator (6 MHz) placed in a closed chamber in which the pressure of water vapor can be set in a range from vacuum ( $<100 \text{ Pa}$ ) up to 80% of water steam at  $25^\circ\text{C}$  ( $P_0 = 31.7 \text{ mbar}$ ). Eq. (1) becomes:

$$m_{\text{sorbed}}(\text{RH}\%) = -\frac{\Delta f}{f_q^2} C \cdot \rho_q \cdot S \quad (2)$$

Data acquisition consisted in collecting the frequency variation due to the sorption of water on cellulose particles adsorbed on the gold surface of the quartz as a function of water vapor pressure and time. Cellulose particles were dried and desorbed at  $25^\circ\text{C}$  during 30 min before sorption kinetics by using a vacuum pumping system composed of a primary dry pump and a turbomolecular pump. Eight successive steps of constant relative humidity were then applied up to 80 %RH (step duration of 10 min). Raw data were converted into mass uptakes as a function of relative humidity by using equation 2. Measurements were done in 6 replicates, corresponding to 6 samples of cellulose deposited on 6 different quartz substrates. Moisture sorption isotherms were determined from the equilibrium moisture contents at each relative humidity step.

### 2.2.2. Particle size and morphology

**Laser granulometry.** The particle size distribution was obtained using a laser diffraction granulometry analyzer (Mastersizer 2000, Malvern Instruments Ltd, U.K.). Approximately 10 mg of cellulose particles were suspended in 50 mL of ethanol 95%. This suspension was added into the experimental cell containing ethanol until reaching an obscuration value between 5% and 10%. Agitation in the cell was set at 3000 rpm and ultra-sounds were used to limit particles agglomeration. Analysis was performed by using refractive indexes of 1.47 and 1.36 for cellulose and ethanol, respectively. Apparent diameter and volume of particle were characterized from the volume diameter distribution. Measurements were done in triplicate.

**Scanning electron microscopy (SEM).** Scanning electron microscopy (SEM) observations were performed with a high-resolution field emission gun (SEM S-4800, Hitachi, Japan) with an acceleration voltage of 2 kV. Prior to SEM analysis, the quartz substrate covered with cellulose particles was coated with a thin layer of platinum in order to avoid sample charging anomalies. This microscopy allows to obtain qualitative information on state of dispersion of cellulose on quartz on the shape of particle.

**Optical microscopy.** Imaging was performed by using a macroscope Multizoom AZ100 (Nikon, Japan) equipped with a RGB DS-Ri1 camera (Nikon, Japon) in light transmission mode. In order to reduce agglomeration of particles, the use of a diluted suspension of cellulose particles in ethanol (concentration of  $0.35 \text{ g.L}^{-1}$ ) was preferred to a direct spray of particles.  $40 \mu\text{L}$  of the cellulose suspension were deposited on each microscope glass slide and then placed in a vacuum chamber to evaporate ethanol. The magnification was set to x32 combining the lens AZ-Plan x4 and setting the optical zoom to x8. For each sample, mosaic images were assembled by reconstructing  $10 \times 4$  images using the imaging software NIS-Elements (Nikon, Japon) operating with the Multizoom AZ100 system.

**Image analysis.** Quantitative morphological parameters were assessed by image analysis. Images obtained from optical microscopy were imported to ImageJ for image processing in order to get the area (number of pixels that represents one cellulose particle multiplied by the resolution), the perimeter (length of the line that delimits the contour of a particle), the major axis (length of the inertia ellipse) and the minor axis (width of the inertia ellipse) of each particle. Image analysis was performed on an increasing number of particles, until the mean of the considered indicator stabilized, *i.e.* with a variation lower than 5%. In our case, the mean was obtained with 120 particles and image analysis was done on 830 particles. Frequency distribution in number and volume of apparent diameter were represented for comparison with light diffraction analysis.

Particle circularity was calculated by Eq. (3):

$$\text{Circularity} = \frac{4\pi \cdot \text{area}}{\text{perimeter}^2} \quad (3)$$

This shape indicator ranges from 0 to 1 (1 for a disc) and allows to know if considered particles are of spherical shape (Lehmann & Legland, 2012).

### 2.2.3. Modeling

Two models were considered to describe water vapor diffusion in a cellulose particle: diffusion in a sphere and in a finite cylinder. Diffusion was assumed to be isotropic and independent of time and position in the material. Analytical solutions provided by Crank (Crank, 1975) were used to perform estimation of diffusivity and equilibrium mass.

#### Case of a homogeneous sphere (radial diffusion)

Under an assumption of homogenous cellulose sphere, water vapor diffusion reduces to a pure radial form. The diffusion equation in a sphere of radius  $R$  (m) for a compound of concentration  $C(t, r)$ , at time  $t$  (s) and radial position  $r$  (m), was then described by Eq. (4).

$$\frac{\partial C}{\partial t}(t, r) = D \left( \frac{\partial^2 C}{\partial r^2} + \frac{2}{r} \frac{\partial C}{\partial r} \right) \quad (4)$$

where  $D$  is the constant diffusivity ( $\text{m}^2 \cdot \text{s}^{-1}$ ).

In this case, we assumed that initial concentration  $C_0$  is uniform and that sample surface is kept at a constant concentration  $C_\infty$  during the experiment:

$$\begin{aligned} C(t=0, r) &= C_0 \quad \forall r \in [0, R] \\ C(t, r=R) &= C_\infty \quad \forall t \geq 0 \end{aligned} \quad (5)$$

For these initial and boundary conditions, the analytical solution is given in Eq. (6), and applies to sphere particles:

$$\frac{M_t}{M_\infty} = 1 - \frac{6}{\pi^2} \sum_{n=1}^{\infty} \frac{1}{n^2} \exp\left(\frac{-Dn^2\pi^2 t}{R^2}\right) \quad (6)$$

where  $M_t$  is the mass uptake ( $\mu\text{g}$ ) at time  $t$  and  $M_\infty$  is the corresponding value for infinite time.

### Case of a homogeneous finite cylinder (axial and radial diffusion)

Considering a homogeneous finite cylinder, diffusion reduces to radial and axial parts. The finite cylinder of radius  $R$  (m) and length  $L$  (m) is defined by  $(r, z) \in [0, R] \times \left[-\frac{L}{2}, \frac{L}{2}\right]$ . The diffusion equation in this finite cylinder, for a compound of concentration  $C(t, r, z)$ , at time  $t$  (s) and spatial position  $(r, z)$ , is given in Eq. (7)

$$\frac{\partial C}{\partial t}(t, r, z) = D \left( \frac{1}{r} \frac{\partial C}{\partial t} + \frac{\partial^2 C}{\partial r^2} + \frac{\partial^2 C}{\partial z^2} \right) \quad (7)$$

where  $D$  is the constant diffusivity ( $\text{m}^2 \cdot \text{s}^{-1}$ ).

As for the spherical geometry, assumptions of uniform initial concentration  $C_0$  and constant concentration  $C_\infty$  at the cylinder surface were made, leading to the following initial and boundary conditions for Eq. (8):

$$\begin{aligned} C(t=0, r, z) &= C_0 \quad \forall (r, z) \in [0, R] \times \left[-\frac{L}{2}, \frac{L}{2}\right] \\ C(t, r=R, z) &= C_\infty \quad \forall t \geq 0 \text{ and } z \in \left[-\frac{L}{2}, \frac{L}{2}\right] \\ C(t, r, z = \pm L/2) &= C_\infty \quad \forall t \geq 0 \text{ and } r \in [0, R] \end{aligned} \quad (8)$$

The finite cylinder of radius  $R$  and length  $L$  is the intersection of an infinite cylinder of the same radius  $R$  and an orthogonal infinite plane sheet of thickness equal to the length  $L$ . Consequently, the analytical solution for this finite cylinder can be written as product of solutions for the radial part, of diffusion, i.e. in the infinite cylinder, and the axial part of the diffusion, i.e. in the infinite plane sheet, as described in Eq. (9) (Afkine & Weber, 2001; J. Matthews & Walker, 1970):

$$\frac{M_t}{M_\infty} \Big|_{\text{Fin. cylinder } (R,L)} = 1 - \left( 1 - \frac{M_t}{M_\infty} \Big|_{\text{Inf. cylinder } (R)} \right) \times \left( 1 - \frac{M_t}{M_\infty} \Big|_{\text{Inf. plane } (L)} \right) \quad (9)$$



$\frac{M_t}{M_\infty} \Big|_{Inf.cylinder (R)}$  is the analytical solution for diffusion in an infinite cylinder of radius R, with the following conditions:

$$\begin{aligned} C(t = 0, r) &= C_0 \forall r \in [0, R] \\ C(t, r = R) &= C_\infty \forall t \geq 0 \end{aligned} \quad (10)$$

It was given by Crank as Eq. (11),

$$\frac{M_t}{M_\infty} \Big|_{Inf. cylinder (R)} = 1 - 4 \sum_{n=1}^{\infty} \frac{\exp(-Dq_n^2 t)}{R^2 q_n^2} \quad (11)$$

where  $q_n$  are the positive roots of the Eq. (12) where  $J_0$  is the Bessel function of the first kind of order 0.

$$J_0(R q_n) = 0 \quad (12)$$

Similarly,  $\frac{M_t}{M_\infty} \Big|_{Inf.plane (L)}$  is the analytical solution for an infinite plane sheet of thickness L (m),

described by  $z \in \left[-\frac{L}{2}, \frac{L}{2}\right]$ , and was also described by Crank as Eq. (14), for the following conditions:

$$\begin{aligned} C(t = 0, z) &= C_0 \forall z \in \left[-\frac{L}{2}, \frac{L}{2}\right] \\ C(t, z = \pm L/2) &= C_\infty \forall t \geq 0 \end{aligned} \quad (13)$$

$$\frac{M_t}{M_\infty} \Big|_{Inf plane (L)} = 1 - 8 \sum_{n=0}^{\infty} \frac{1}{(2n+1)^2 \pi^2} \exp\left(\frac{-D(2n+1)^2 \pi^2 t}{L^2}\right) \quad (14)$$

### Numerical simulations and parameter estimation

Parameter estimation resumes to a nonlinear least squares problem. Error between experimental and predicted kinetics was described by the root mean squared error, RMSE, given in Eq. (15).

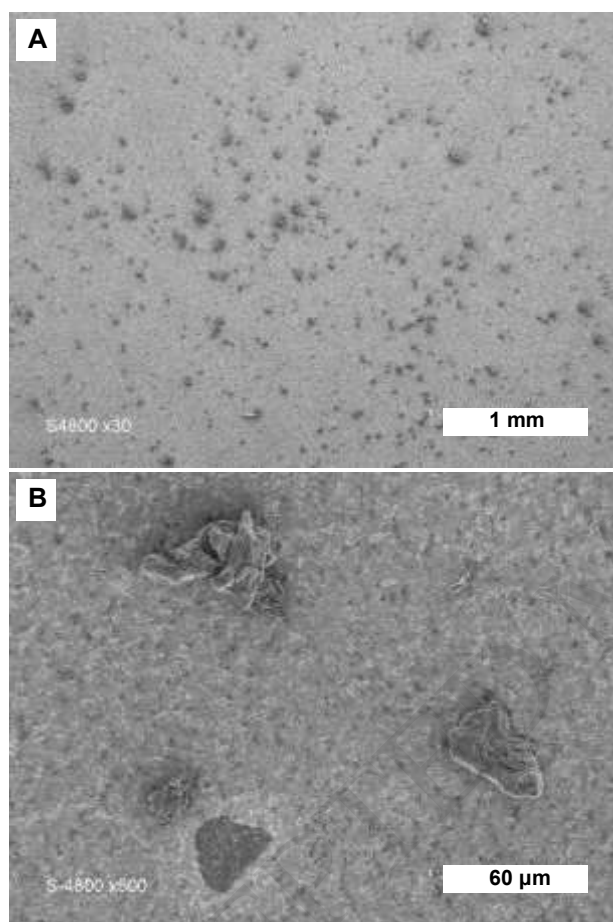
$$RMSE = \sqrt{\frac{\sum_{i=1}^N (m_{sim}(t_i) - m_{exp}(t_i))^2}{N}} \quad (15)$$

where  $m_{sim}(t_i)$  is the mass predicted at time  $t_i$ ,  $m_{exp}(t_i)$  is the experimental data of mass uptake at time  $t_i$  and N is sample size. Finally, numerical simulations were performed by using Matlab<sup>®</sup> software and using its *lsqnonlin* function for estimation of apparent diffusivity and equilibrium mass.

## 3. Results and discussion

### 3.1. Water vapor sorption kinetics

Preliminary to water vapor sorption kinetics, SEM observations of the quartz substrates, on which 1 to 1.5  $\mu\text{g}$  of cellulose particles were adsorbed, were carried out to evaluate the dispersion state of the particles. It was shown that cellulose particles were well dispersed on the surface of the quartz, without any visible agglomeration phenomena (Fig. 1). This observation confirmed that recorded water vapor sorption kinetics occurred at the scale of individual particles and not at the scale of agglomerates of particles.



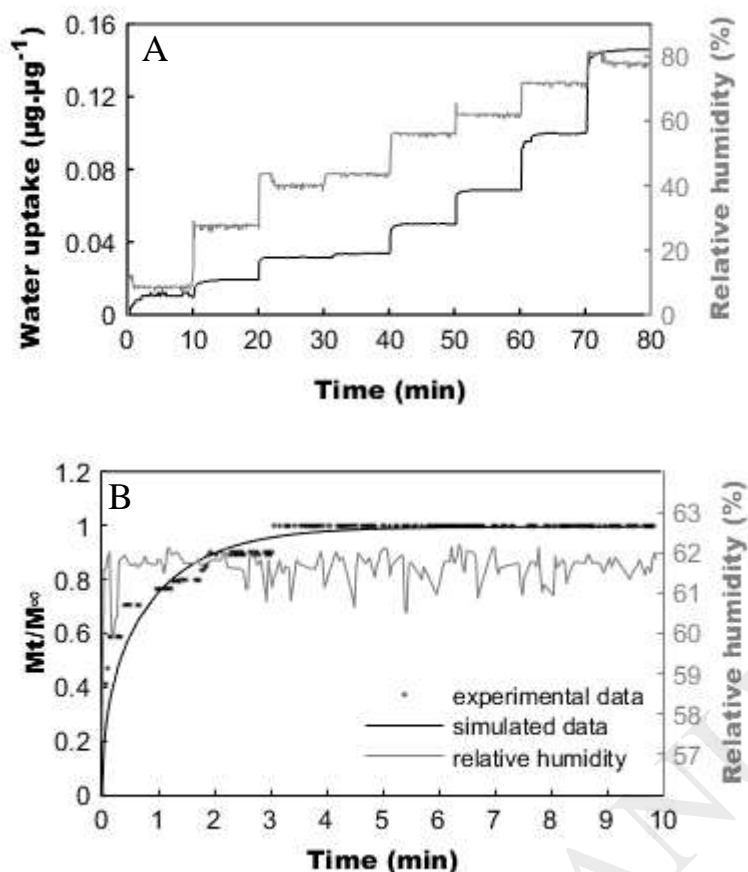
**Fig. 1** SEM images of cellulose particles adsorbed on a quartz substrate at magnitudes of (A) x30 and (B) x500.

Fig. 2A presents the evolution of water vapor uptake as a function of time for 8 successive steps of relative humidity (RH). Results showed classical sorption curves displaying no significant artefacts, thus suggesting that estimation of diffusion and sorption parameters will be possible. It was checked that no particle fell down of the quartz support during the experiment, even at high relative humidity. To control that, after each sorption kinetics step, water vapor pressure was decreased down to 0 Pa (pumped down to the limit vacuum) during 30 minutes to desorb water (the frequency equilibrium was reached again after a maximum duration of 15 min). It was shown that the quartz frequency after this

desorption step was the same as the initial one, which allows concluding that the weight of dried cellulose remained constant. As compared to other methods, the QCM methodology is very fast, e.g. 8 steps of RH achieved after 80 min, and used little quantities of sample (between 1 and 1.5  $\mu\text{g}$  on each substrate).

The only drawback of this QCM setup is the difficulty to control the targeted RH value at each step. However, what is important is that when the introduction gate is closed, the water vapor pressure is very stable. Finally, it was assumed in the present study that energy dissipation phenomena in cellulose particles did not occur over the range of studied relative humidity (0-80 %RH) (Hakalahti et al., 2017; Tammelin et al., 2015). As an example, no significant dissipation was registered for RH lower or equal to 75%RH in the work of Hakalahti et al. on cellulose nanofibrils films (Hakalahti et al., 2017). However, we cannot ensure that micrometric size particles, which are not covering the whole surface of the substrate, are behaving the same manner as a continuous and homogeneous film. Further experiments should be carried out using the QCM-D technique to valid the fact that dissipation would not increase significantly at high RH in micrometric size cellulose particles and thus become an issue in the proposed methodology.

It was checked that mass equilibrium was reached after less than 4 min, which allows considering as pertinent a duration of every step of 10 min. It was also verified that the RH equilibrium was reached faster than the mass equilibrium, which makes possible to assume constant RH over the all duration of the step in the modeling approach (Figure 2B). Water vapor apparent diffusivity,  $D$ , and sorption at equilibrium,  $M_{\infty}$ , were estimated at each RH step using analytical solutions of diffusion equation presented in section 2.2.2 (Eq. (6) and (9)). The inputs for the estimation of these parameters were the kinetics of water vapor uptake as a function of time, the geometry and the dimensions of the particles. Fig. 2B displays an example of comparison between experimental and simulated data for a RH step from 56% to 62% by considering the cylinder model. Following estimated parameters were obtained:  $D = 7.6 \times 10^{-13} \text{ m}^2 \cdot \text{s}^{-1}$  and  $M_{\infty} = 0.0732 \text{ } \mu\text{g} \cdot \mu\text{g}^{-1} \text{ d.b.}$  (dry basis) (experimental  $M_{\infty} = 0.0730 \text{ } \mu\text{g} \cdot \mu\text{g}^{-1} \text{ d.b.}$ ). It could be noted that the model used correctly fit experimental data with an RMSE equal to 0.005  $\mu\text{g} \cdot \mu\text{g}^{-1}$  and determination coefficient  $R^2 = 0.91$ .



**Fig. 2** (A) Example of water vapor sorption kinetics of cellulose: black curve shows water uptake ( $\mu\text{g}$ ) and grey curve corresponds to relative humidity (%). (B) Example of simulation on one step of relative humidity (from 56% to 62%).

### 3.2. Morphological analysis: sphere vs. cylinder shaped particles

The choice of the analytical solution that will be used to estimate diffusivity and water uptake at  $M_{\infty}$  from water vapor sorption kinetics is based on the geometry of particles. It is very critical since it can significantly impact the estimated values. Consequently, an accurate determination of morphological parameters of studied particles was necessary, at least to determine their shape. For that purpose, SEM observations were done in a first approach to qualitatively assess the shape of particles. It was shown that the cellulose sample was characterized by a polydispersity of both sizes and shapes, with either sphere-like, ribbon-like or cylinder-like shapes and sizes ranging from 2  $\mu\text{m}$  up to 60  $\mu\text{m}$  (Fig. 3). A first approximation could be to consider that particles are spherical. Hence, using laser granulometry to better assess the size distribution of the cellulose sample was considered as correct.

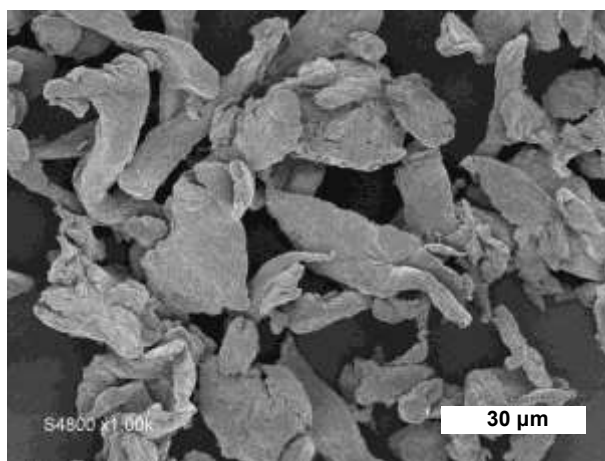


**Fig. 3** SEM image of cellulose particles.

Monomodal number- and volume-based particle size distributions were obtained by laser granulometry. The number-based distribution gives more importance to small particles while the volume-based distribution places greater prominence to big particles. In our case, since cellulose particles are dedicated to be used as fillers in composite materials, with a special focus on mass transfer properties, we considered that it was more pertinent to consider volume-based descriptors for the rest of the study. Indeed, models proposed to formalize structure/mass transfer properties in composite materials are all using the volume filler content as input parameter (Wolf et al., 2016). Furthermore, the consideration of number-based descriptors, e.g. mean, median or mode, would underestimate the volume (and therefore the mass) of the particles, which would induce errors on the estimated diffusivity. The median equivalent diameter in volume was  $20.1 \pm 0.1 \mu\text{m}$  with a span value (representing the spreading of the distribution) of  $2.0 \pm 0.1 \mu\text{m}$ .

Quantitative morphological parameters of cellulose particles were obtained from image analysis and are summarized in Table 1. Two dimensions were considered, *i.e.* a long length (major axis) and a small length (minor axis). Median values in volume of dimensions were  $30.7 \mu\text{m}$  and  $18.2 \mu\text{m}$ , respectively. The average circularity of cellulose particles was  $0.8 \pm 0.2$ , allowing to conclude that the assumption of spherical particles did not perfectly represent the reality. The elongation value, corresponding to the ratio between the maximal dimension (major axis) and the minimal dimension (minor axis), was  $1.5 \pm 0.2$  showing that particles were slightly elongated. However, as shown on Fig. 4, it is worth noting that 34% in number of particles had a circularity very close to 1 and even so can be considered as spherical. On this figure, a part of particles had a circularity higher than 1, it can be explained by discretization errors done by Image J software (Lehmann & Legland, 2012). It could be deduced from these results that particles should be better assimilated to finite cylinders instead of

spheres. It was thus assumed that the major axis corresponded to the length of the cylinder,  $L$ , and the minor axis to the diameter of the cylinder,  $d=2R$ .

**Table 1.** Particle morphological parameters obtained by granulometry and image analysis. Numbers in brackets refer to span values (the span value represents the difference between the 90<sup>th</sup> and 10<sup>th</sup> percentiles divided by the median value).

	Laser granulometry		Image analysis	
	Median diameter (span) in $\mu\text{m}$	Median major axis (span) in $\mu\text{m}$	Median minor axis (span) in $\mu\text{m}$	Median circularity
Number-based distributions	$7.4 \pm 0.2$ (1.5)	$19 \pm 1$ (2.1)	$11 \pm 1$ (1.5)	0.8
Area-based distributions	$13.2 \pm 0.1$ (1.8)	$25 \pm 2$ (1.5)	$15 \pm 1$ (1.1)	-
Volume-based distributions	$20.1 \pm 0.1$ (2.0)	$31 \pm 2$ (1.4)	$18 \pm 1$ (0.9)	-

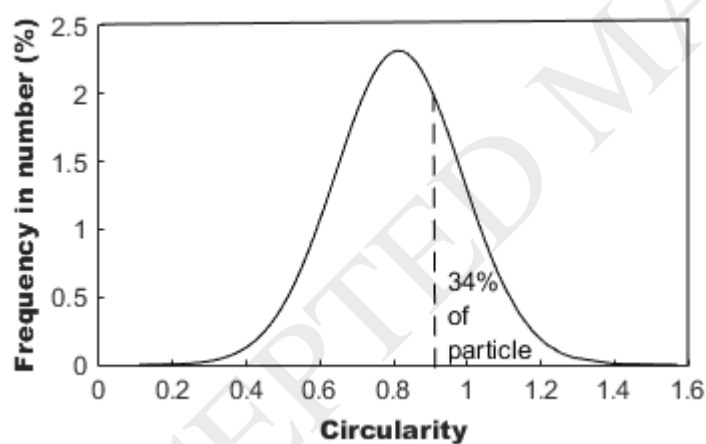


**Fig. 4** Number based circularity distribution of cellulose particles

### 3.3. Water vapor sorption isotherm

Fig. 5 displays sorption isotherm curves for micrometric size cellulose particles. Isotherms displayed a sigmoid shape, as already reported (Nelson, 1983; Paes et al., 2010). A good repeatability was obtained by considering an initial weight of absorbed cellulose ranging from 1 to 1.5  $\mu\text{g}$  and by taking care of depositing cellulose only on the usable surface of the quartz substrate. Water vapor uptake varied from 0.142 to 0.148  $\mu\text{g} \cdot \mu\text{g}^{-1}$  d.b. at 78 % of RH (Fig. 5). In this case, some values were higher

than some already published data, e.g. a water uptake of  $0.1 \text{ g.g}^{-1} \text{ d.b.}$  for microcrystalline cellulose particle (size superior of  $63 \mu\text{m}$ ) at 75 % of RH (Kachrimanis, Noisternig, Griesser, & Malamataris, 2006), or around  $0.18 \text{ g.g}^{-1} \text{ d.b.}$  at 75% of RH for balled milled cellulose (Paes et al., 2010). Such discrepancy could be explained by the fact that cellulose particles considered in the present study were quasi amorphous, with a crystallinity value lower than 5 %. Indeed, as already demonstrated, the more the cellulose is amorphous, the more the water sorption will be favored since sorption occurs mainly in amorphous regions of a semi-crystalline material (Mihriyan et al., 2004).

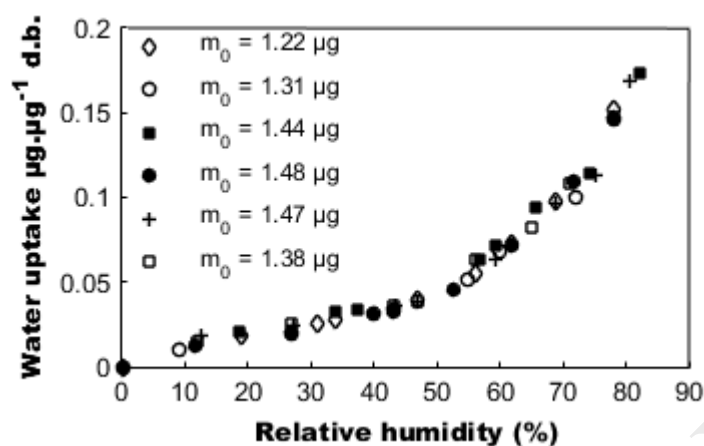


Fig. 5 Water vapor sorption isotherms of cellulose particles.

### 3.4. Water vapor diffusivity identification

Based on image analysis results, water vapor diffusivity in micrometric size cellulose particles was estimated by considering either a spherical or a cylindrical geometry. In the case of a sphere, a radius value  $R$  of  $10.1 \mu\text{m}$  was considered (half median diameter), provided by laser granulometry analysis. In the case of the cylindrical geometry, a radius  $R$  of  $9.1 \mu\text{m}$  (half median minor axis) and a length  $L$  of  $30.7 \mu\text{m}$  (median major axis) were taken (Table 1).

Results of water vapor apparent diffusivity estimated by sphere and cylinder models in cellulose were presented on Fig. 6. Same values of water vapor diffusivity were estimated by taking into consideration either the spherical Eq. (6), or the cylindrical Eq. (9), geometry. A cloud of points for 6 samples was obtained, with diffusivity ranging from  $2.4 \times 10^{-14} \text{ m}^2.\text{s}^{-1}$  to  $4.2 \times 10^{-12} \text{ m}^2.\text{s}^{-1}$  and an average value equal to  $8.4 \times 10^{-13} \pm 8.6 \times 10^{-13} \text{ m}^2.\text{s}^{-1}$  (for the cylinder geometry). This dispersion could be explained by variations in the length of RH steps depending on each step and each sample. Since water vapor diffusivity has never been estimated for micrometric size particles, our results can only be compared to values obtained for cellulose-based films. Our values were in a range of diffusivity estimated for microcrystalline cellulose films, i.e. from  $3 \times 10^{-14} \text{ m}^2.\text{s}^{-1}$  to  $2 \times 10^{-13} \text{ m}^2.\text{s}^{-1}$  (Bedane, Eić, Farmahini-Farahani, & Xiao, 2015). Observed differences could be explained by the nature of sample,

i.e. either powder or films. At the macroscopic scale of films, undesirable phenomena could occur without being taken into account in models. It includes porosity effect (water vapor diffusivity in pores omitted), swelling of materials with increasing water content (modification of structure), or aggregation/agglomeration of nanofibrils. The use of the QCM system allows reducing these possible negative effects for the estimation of diffusivity by working on the scale of individual micrometric size particles.

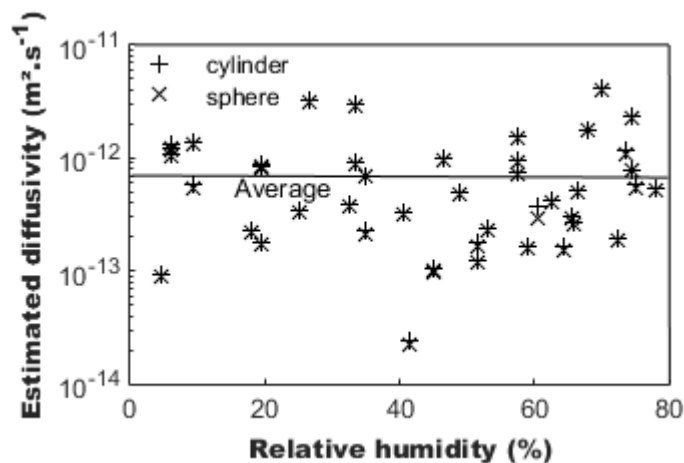


**Fig. 6** Estimated water vapor diffusivities of cellulose particles for different relative humidity. Cylinder diffusivity average =  $8.4 \times 10^{-13} \pm 8.6 \times 10^{-13} \text{ m}^2 \cdot \text{s}^{-1}$  and sphere diffusivity average =  $8.0 \times 10^{-13} \pm 8.2 \times 10^{-13} \text{ m}^2 \cdot \text{s}^{-1}$

### 3.5. Cylinder vs. sphere modeling approach

Section 3.4 showed that both cylinder and sphere geometries led to the same values of estimated diffusivities. The question of the validity of this conclusion for longer particles must be discussed. For that purpose, a confrontation between sphere and cylinder models was done. Simulated data of water uptake were generated by cylinder model for different values of elongation  $e=L/(2R)$  by considering constant values of radius ( $R$ ) and diffusivity ( $D_0$ ). For each elongation, these data were then used as inputs in the sphere model to estimate diffusivity ( $D^*$ ), setting the radius of the sphere in such a way to preserve the particle volume. Relative error  $\text{err}=(D_0-D^*) \cdot D_0^{-1}$  was represented as a function of the cylinder elongation. Results showed the same trend whatever the value set for the radius of cylinder (Fig. 7). Consequently, it was deduced that this parameter (radius) had no impact for comparison between these two models and same trend was observed with  $D_0$  parameter (by testing 3 different diffusivities:  $10^{-12}$ ,  $10^{-14}$  and  $10^{-16} \text{ m}^2 \cdot \text{s}^{-1}$ ). For an elongation equal to 1.5 (case of this study), the relative error was around 5.5%, confirming that the two models could be used indifferently. Considering that 15% is an acceptable value of relative error, a critical elongation value of 2 could be



estimated. This means that for elongation values lower than 2, cylindrical particles can be assimilated as spherical particles while for elongation higher than 2, cylinder geometry must be considered.

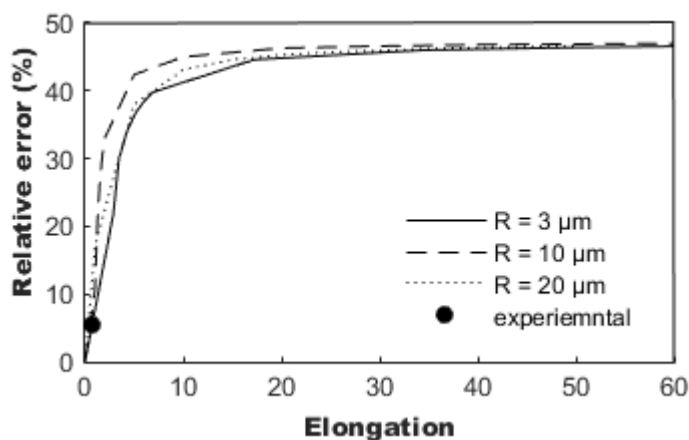


**Fig. 7** Relative error between cylinder model and sphere model for different values of elongation.

□ corresponds to the error for the cylinder and sphere dimensions used in the current work.

#### 4. Conclusion

The study demonstrated the capacity of the quartz crystal microbalance coupled with an adsorption system to evaluate water vapor transfers in micrometric size cellulose particles. The huge advantage of this technique is the possibility of working on very little quantities of sample, i.e. 1 μg, thus permitting to estimate parameters at the scale of individual particles. This allows avoiding edge effects such as agglomeration, swelling or percolation. The QCM is also a very fast method as compared to others, with a total acquisition duration of the order of one hour. It was shown that the QCM methodology is adapted to obtain moisture isotherm for a sample weight ranging from 1 to 1.5 μg and by taking care of depositing cellulose only on the usable surface of the quartz substrate. It is worth noting that the proposed methodology should be corroborated by monitoring energy dissipation using the QCM-D technique and checking that dissipation would not significantly increase with increasing RH. From water vapor sorption isotherm and using modeling tools (analytical solution of sphere or finite cylinder), water vapor diffusivity of amorphous cellulose particles was estimated at different relative humidity. Estimated diffusivity was not significantly impacted by the relative humidity, with an average value of  $8 \times 10^{-13} \text{ m}^2 \cdot \text{s}^{-1}$ . It was shown that a finite cylinder or spherical geometry could be used equally for diffusivity identification for a particle size aspect ratio lower than 2. For size aspect ratio higher than 2, a cylinder geometry should be considered.

#### 5. Acknowledgements

Direct costs were covered by the MALICE project (call “Chercheur d’avenir 2015”), which is co-financed by the European Regional Development Fund (FEDER) and the Languedoc-Roussillon region.

## 6. References

Afkin, G. B., & Weber, H. J. (2001). *Mathematical Methods for Physicists*.

Ahola, S., Myllytie, P., Österberg, M., Teerinen, T., & Laine, J. (2008). EFFECT OF POLYMER ADSORPTION ON CELLULOSE NANOFIBRIL WATER BINDING CAPACITY AND AGGREGATION. *BioResources*, 3(4), 1315–1328.  
<https://doi.org/10.15376/biores.3.4.1315-1328>

Bedane, A. H., Eić, M., Farmahini-Farahani, M., & Xiao, H. (2015). Water vapor transport properties of regenerated cellulose and nanofibrillated cellulose films. *Journal of Membrane Science*, 493, 46–57. <https://doi.org/10.1016/j.memsci.2015.06.009>

Bedane, A. H., Huang, Q., Xiao, H., & Ei, M. (2012). Mass transfer of water vapor, carbon dioxide and oxygen on modified cellulose fiber-based materials. *Nordic Pulp and Paper Research Journal*, 27(2), 409.

Berthet, M.-A., Angellier-Coussy, H., Guillard, V., & Gontard, N. (2016). Vegetal fiber-based biocomposites: Which stakes for food packaging applications? *Journal of Applied Polymer Science*, 133(2), n/a-n/a. <https://doi.org/10.1002/app.42528>

Berthet, M.-A., Gontard, N., & Angellier-Coussy, H. (2015). Impact of fibre moisture content on the structure/mechanical properties relationships of PHBV/wheat straw fibres biocomposites. *Composites Science and Technology*, 117, 386–391.  
<https://doi.org/10.1016/j.compscitech.2015.07.015>

Bessadok, A., Langevin, D., Gouanvé, F., Chappey, C., Roudesli, S., & Marais, S. (2009). Study of water sorption on modified Agave fibres. *Carbohydrate Polymers*, 76(1), 74–85. <https://doi.org/10.1016/j.carbpol.2008.09.033>

- Caron, T., Pasquinet, E., van der Lee, A., Pansu, R. B., Rouessac, V., Clavaguera, S., ...  
Montméat, P. (2014). Efficient Sensing of Explosives by Using Fluorescent  
Nonporous Films of Oligophenyleneethynylene Derivatives Thanks to Optimal  
Structure Orientation and Exciton Migration. *Chemistry – A European Journal*,  
20(46), 15069–15076. <https://doi.org/10.1002/chem.201402271>
- Céline, A., Fréour, S., Jacquemin, F., & Casari, P. (2013). Characterization and modeling of  
the moisture diffusion behavior of natural fibers. *Journal of Applied Polymer Science*,  
130(1), 297–306. <https://doi.org/10.1002/app.39148>
- Crank, J. (1975). *The mathematics of diffusion*.
- de Carvalho, L. H., Barbosa de Lima, A. G., Canedo, E. L., Bezerra, A. F. C., Cavalcanti, W.  
S., & Marinho, V. A. D. (2016). Water Sorption of Vegetable Fiber Reinforced  
Polymer Composites. *Defect and Diffusion Forum*, 369, 17–23.  
<https://doi.org/10.4028/www.scientific.net/DDF.369.17>
- Gouanvé, F., Marais, S., Bessadok, A., Langevin, D., & Métayer, M. (2007). Kinetics of  
water sorption in flax and PET fibers. *European Polymer Journal*, 43(2), 586–598.  
<https://doi.org/10.1016/j.eurpolymj.2006.10.023>
- Gouanvé, F., Marais, S., Bessadok, A., Langevin, D., Morvan, C., & Métayer, M. (2006).  
Study of water sorption in modified flax fibers. *Journal of Applied Polymer Science*,  
101(6), 4281–4289. <https://doi.org/10.1002/app.23661>
- Guillard, V., Broyart, B., Bonazzi, C., Guilbert, S., & Gontard, N. (2003). Moisture  
Diffusivity in Sponge Cake as Related to Porous Structure Evaluation and Moisture  
Content. *Journal of Food Science*, 68(2), 555–562. <https://doi.org/10.1111/j.1365-2621.2003.tb05711.x>
- Hakalahti, M., Faustini, M., Boissière, C., Kontturi, E., & Tammelin, T. (2017). Interfacial  
Mechanisms of Water Vapor Sorption into Cellulose Nanofibril Films as Revealed by

Quantitative Models. *Biomacromolecules*, 18(9), 2951–2958.

<https://doi.org/10.1021/acs.biomac.7b00890>

Hashemi, S. J., Comes, V. G., Crotogino, R. H., & Douglas, W. J. M. (1997). In-Plane

Diffusivity of Moisture in Paper. *Drying Technology*, 15(2), 265–294.

<https://doi.org/10.1080/07373939708917234>

J. Matthews, & Walker, R. L. (1970). *Mathematical Methods of Physics*.

Jia, Y., Yu, H., Zhang, Y., Dong, F., & Li, Z. (2016). Cellulose acetate nanofibers coated layer-by-layer with polyethylenimine and graphene oxide on a quartz crystal microbalance for use as a highly sensitive ammonia sensor. *Colloids and Surfaces B: Biointerfaces*, 148, 263–269. <https://doi.org/10.1016/j.colsurfb.2016.09.007>

Kachrimanis, K., Noisternig, M., Griesser, U., & Malamataris, S. (2006). Dynamic moisture sorption and desorption of standard and silicified microcrystalline cellulose. *European Journal of Pharmaceutics and Biopharmaceutics*, 64(3), 307–315.

<https://doi.org/10.1016/j.ejpb.2006.05.019>

Khazaei, J. (2008). Water absorption characteristics of three wood varieties. *Cercetări Agronomice În Moldova*, 41(2), 134.

Kontturi, K. S., Kontturi, E., & Laine, J. (2013). Specific water uptake of thin films from nanofibrillar cellulose. *Journal of Materials Chemistry A*, 1(43), 13655–13663.

<https://doi.org/10.1039/C3TA12998E>

Kushner, D. I., & Hickner, M. A. (2017). Water Sorption in Electron-Beam Evaporated SiO<sub>2</sub> on QCM Crystals and Its Influence on Polymer Thin Film Hydration Measurements.

*Langmuir*, 33(21), 5261–5268. <https://doi.org/10.1021/acs.langmuir.7b00759>

Lehmann, G., & Legland, D. (2012). *Efficient N-Dimensional surface estimation using Crofton formula and run-length encoding*.

- Li, T.-Q., Henriksson, U., Klason, T., & Ödberg, L. (1992). Water diffusion in wood pulp cellulose fibers studied by means of the pulsed gradient spin-echo method. *Journal of Colloid and Interface Science*, 154(2), 305–315. [https://doi.org/10.1016/0021-9797\(92\)90145-C](https://doi.org/10.1016/0021-9797(92)90145-C)
- Marais, S., Nguyen, Q. T., Devallencourt, C., Metayer, M., Nguyen, T. U., & Schaezel, P. (2000). Permeation of water through polar and nonpolar polymers and copolymers: Determination of the concentration-dependent diffusion coefficient. *Journal of Polymer Science Part B: Polymer Physics*, 38(15), 1998–2008. [https://doi.org/10.1002/1099-0488\(20000801\)38:15<1998::AID-POLB50>3.0.CO;2-A](https://doi.org/10.1002/1099-0488(20000801)38:15<1998::AID-POLB50>3.0.CO;2-A)
- Marx, K. A. (2003). Quartz Crystal Microbalance: A Useful Tool for Studying Thin Polymer Films and Complex Biomolecular Systems at the Solution–Surface Interface. *Biomacromolecules*, 4(5), 1099–1120. <https://doi.org/10.1021/bm020116i>
- Mecea, V. M. (2006). Is quartz crystal microbalance really a mass sensor? *Sensors and Actuators A: Physical*, 128(2), 270–277. <https://doi.org/10.1016/j.sna.2006.01.023>
- Michalzik, M., Wilke, R., & Büttgenbach, S. (2005). Miniaturized QCM-based flow system for immunosensor application in liquid. *Sensors and Actuators B: Chemical*, 111, 410–415. <https://doi.org/10.1016/j.snb.2005.03.048>
- Mihrianyan, A., Llagostera, A. P., Karmhag, R., Strømme, M., & Ek, R. (2004). Moisture sorption by cellulose powders of varying crystallinity. *International Journal of Pharmaceutics*, 269(2), 433–442. <https://doi.org/10.1016/j.ijpharm.2003.09.030>
- Minelli, M., Giancinti Baschetti, M., Doghieri, F., Ankerfors, M., Lindström, T., Siro, I., & Plackett, D. (2010). Investigation of mass transport properties of MFC films. *Journal of Membrane Science*, 358, 67–75.

- Nelson, R. M. (1983). A Model for Sorption of Water Vapor by Cellulosic Materials, *15*(1), 8–22.
- Niinivaara, E., Faustini, M., Tammelin, T., & Kontturi, E. (2015). Water Vapor Uptake of Ultrathin Films of Biologically Derived Nanocrystals: Quantitative Assessment with Quartz Crystal Microbalance and Spectroscopic Ellipsometry. *Langmuir: The ACS Journal of Surfaces and Colloids*, *31*(44), 12170–12176.  
<https://doi.org/10.1021/acs.langmuir.5b01763>
- Niinivaara, E., Faustini, M., Tammelin, T., & Kontturi, E. (2016). Mimicking the Humidity Response of the Plant Cell Wall by Using Two-Dimensional Systems: The Critical Role of Amorphous and Crystalline Polysaccharides. *Langmuir*, *32*(8), 2032–2040.  
<https://doi.org/10.1021/acs.langmuir.5b04264>
- Nilsson, L., Wilhelmsson, B., & Stenstrom, S. (1993). THE DIFFUSION OF WATER VAPOUR THROUGH PULP AND PAPER. *Drying Technology*, *11*(6), 1205–1225.  
<https://doi.org/10.1080/07373939308916896>
- Paes, S. S., Sun, S., MacNaughtan, W., Ibbett, R., Ganster, J., Foster, T. J., & Mitchell, J. R. (2010). The glass transition and crystallization of ball milled cellulose. *Cellulose*, *17*(4), 693–709. <https://doi.org/10.1007/s10570-010-9425-7>
- Passamano, M., & Pighini, M. (2006). QCM DNA-sensor for GMOs detection. *Sensors and Actuators B: Chemical*, *118*(1–2), 177–181. <https://doi.org/10.1016/j.snb.2006.04.012>
- Roemhild, K., Niemz, F., Mohan, T., Hribernik, S., Kurecic, M., Ganser, C., ... Spirk, S. (2016). The Cellulose Source Matters—Hollow Semi Spheres or Fibers by Needleless Electrospinning. *Macromolecular Materials and Engineering*, *301*(1), 42–47.  
<https://doi.org/10.1002/mame.201500191>
- Rouessac, V., van der Lee, A., Bosc, F., Durand, J., & Ayrat, A. (2008). Three characterization techniques coupled with adsorption for studying the nanoporosity of

- supported films and membranes. *Microporous and Mesoporous Materials*, 111(1), 417–428. <https://doi.org/10.1016/j.micromeso.2007.08.033>
- Simpson, W. T. (1993). Determination and use of moisture diffusion coefficient to characterize drying of northern red oak (*Quercus rubra*). *Wood Science and Technology*, 27(6), 409–420. <https://doi.org/10.1007/BF00193863>
- Stockbridge, C. D., Warner, A. W., & Behrnt, K. H. (1963). *Vacuum Microbalance Techniques* (Vol. 3). Proceedings of the Los Angeles Conference: Plenum Press.
- Tammelin, T., Abburi, R., Gestranus, M., Laine, C., Setälä, H., & Österberg, M. (2015). Correlation between cellulose thin film supramolecular structures and interactions with water. *Soft Matter*, 11(21), 4273–4282. <https://doi.org/10.1039/C5SM00374A>
- Thomas, E., Rudich, Y., Trakhtenberg, S., & Ussyshkin, R. (1999). Water adsorption by hydrophobic organic surfaces: Experimental evidence and implications to the atmospheric properties of organic aerosols. *Journal of Geophysical Research: Atmospheres*, 104(D13), 16053–16059. <https://doi.org/10.1029/1999JD900196>
- Tiaya Mbou, E., Njeugna, E., Kemajou, A., Sikame, N. R. T., & Ndapeu, D. (2017). Modelling of the Water Absorption Kinetics and Determination of the Water Diffusion Coefficient in the Pith of *Raffia vinifera* of Bandjoun, Cameroon [Research article]. <https://doi.org/10.1155/2017/1953087>
- Villares, A., Moreau, C., Dammak, A., Capron, I., & Cathala, B. (2015). Kinetic aspects of the adsorption of xyloglucan onto cellulose nanocrystals. *Soft Matter*, 11(32), 6472–6481. <https://doi.org/10.1039/c5sm01413a>
- Wolf, C., Guillard, V., Angellier-Coussy, H., Silva, G. G. D., & Gontard, N. (2016). Water vapor sorption and diffusion in wheat straw particles and their impact on the mass transfer properties of biocomposites. *Journal of Applied Polymer Science*, 133(16), n/a-n/a. <https://doi.org/10.1002/app.43329>